Power-Efficient Constellations for Amplified Stokes Vector Detection With Signal-Dependent Noise

Thomas Horton King, *Graduate Student Member, IEEE*, and Joseph M. Kahn, *Life Fellow, IEEE*

***Abstract*—We discuss the design of three-dimensional constellations for amplifier noise-limited Stokes vector detection (ASVD) systems, where amplified spontaneous emission from optical amplifiers is the dominant noise source. We derive a decision statistic, approximate pairwise error probability, and union bound symbol-error ratio, leading to an objective function for designing ASVD constellations. We propose two new methods of designing ASVD constellations, which can be used to generate optimized or practical constellations. We carry out both design methods for constellations with modulation orders of 2, 4, 8, 16, 32, and 64. We simulate the constellations' receiver sensitivities and compare them to existing constellations; for 16-ary and 64-ary constellations respectively, the optimized designs improve sensitivity by 2.02 dB and 1.91 dB, and the practical designs improve sensitivity by 1.29 dB and 1.71 dB. We show that modulating higher-order ASVD constellations can be facilitated by combining amplitude and phase modulation. We study the impact of planar decision boundaries and finite analog-to-digital converter resolution on detection performance, finding a 0.3 dB receiver sensitivity degradation for a 6-bit converter and 16-ary constellation.**

***Index Terms*—Amplified spontaneous emission, constellation design, constellation optimization, direct detection (DD), signal-dependent noise, sphere packing, Stokes vector detection, Stokes vector receiver (SVR), three-dimensional constellations.**

I. Introduction

TO MEET the increasing capacity demands of short reach data center links, there has been much work on detection methods that provide more degrees of freedom than the traditionally used intensity-modulated direct-detection systems [1], [2], [3], [4], [5]. Stokes vector (SV) detection is one such method that utilizes three out of the four available degrees of freedom of single-mode fiber (SMF) without requiring a local oscillator at the receiver [6], [7], [8], [9], [10], [11], [12], [13], [14], [15]. An additional degree of freedom can be encoded in the differential phase between successive symbols, as done in [15]; since this differential phase can be detected separately from the SV, we do not discuss it in detail here.

Received 1 May 2025; revised 1 August 2025; accepted 27 September 2025. Date of publication 6 October 2025; date of current version 16 December 2025. This work was supported in part by Meta through the Stanford Photonics Research Center, in part by the Stanford SystemX Alliance, and in part by a Stanford Graduate Fellowship. *(Corresponding author: Thomas Horton King.)*

The authors are with the E. L. Ginzton Laboratory, Department of Electrical Engineering, Stanford University, Stanford, CA 94305 USA (e-mail: thomashk@stanford.edu; jmk@ee.stanford.edu).

Color versions of one or more figures in this article are available at https://doi.org/10.1109/JLT.2025.3618218.

Digital Object Identifier 10.1109/JLT.2025.3618218

There are two primary noise regimes for SV detection: thermal noise-limited SV detection (TSVD), in which case electrical noise from the transimpedance amplifiers used by the SV receiver is the dominant source of noise, and amplifier noise-limited SV detection (ASVD), in which case amplified spontaneous emission (ASE) from optical amplifiers is the dominant source of noise [16]. There is a third noise regime, quantum noise-limited SV detection [17], but we will not discuss it in this paper. In practice, optical amplification is often required to achieve a high data rate for SV detection since SV receivers have high insertion and splitting losses. Since the magnitude of amplifier noise is typically much larger than that of electrical noise, most SV detection systems fall under the ASVD regime [6], [7], [8], [9], [10], [11], [12], [13], [14], [15].

Despite substantial interest in SV detection, the design of optimal, three-dimensional constellations has only been considered for TSVD in [18] or non-optimally for ASVD in [6]. In this paper, we consider an optimal constellation to be one that minimizes the required average transmitted optical power to achieve a given symbol-error ratio (SER) at a fixed spectral efficiency [19]. Constellation design, especially for channels with non-standard noise characteristics, is a rich area of research. A non-exhaustive list of constellation design methods includes geometry-based methods [6], [18], [19], shell-based methods [20], pairwise algorithms [21], genetic and simulated annealing algorithms [22], [23], and other optimization-based methods [24], [25], [26]. Owing to the signal-dependent noise of ASVD, known constellations are suboptimal, especially at higher modulation orders.

In this paper, we examine constellation design for ASVD. The structure of the paper is as follows. Section II reviews ASVD systems and presents an approximate channel model for ASVD. Section III derives approximate error probabilities for ASVD constellations, defines an objective function for optimizing constellations, and presents a geometrical approach to designing ASVD constellations. Section IV-A discusses an optimization-based technique to design best performing constellations, and Section IV-B discusses a shell-based technique to design more practical constellations. Section V lists the characteristics of previously and newly proposed constellations, and presents simulations to quantify their performance for ASVD. Section VI discusses challenges in implementing higher modulation order constellations for ASVD and explores possible realizations of the modulator and detector structures.

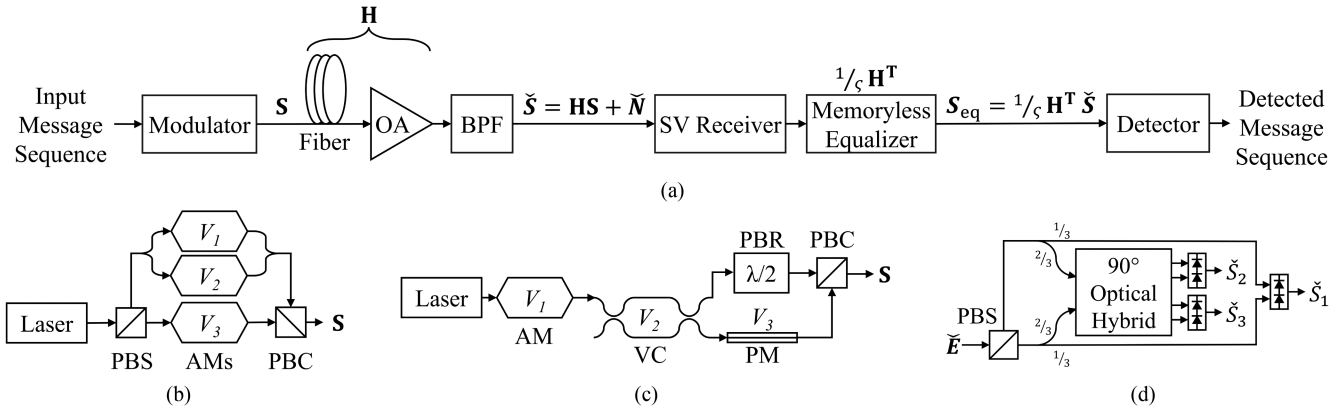

Fig. 1. (a) An end-to-end ASVD system. Two possible structures for the modulator are (b) the dual-polarization in-phase quadrature modulator and (c) the Kikuchi modulator. As explained in the text, only three modulators are needed for the dual-polarization in-phase quadrature modulator. (d) A possible structure for the SV receiver with minimal number of electrical outputs using balanced photodiodes. OA: Optical Amplifier, BPF: Band-pass Filter, SV: Stokes Vector, PBS: polarization beam splitter, PBC: polarization beam combiner, PBR: polarization beam rotator, AM: amplitude modulator, VC: amplitude modulator serving as variable coupler, PM: phase modulator.

II. System Model

This section describes ASVD links and derives an approximate end-to-end channel model.

A. Amplified Stokes Vector Detection

Fully polarized light in SMF can be represented by a Jones vector $\mathbf{E} = [E_1, E_2]^T = [E_{1,I} + jE_{1,Q}, E_{2,I} + jE_{2,Q}]^T$, where E_1 and E_2 are the complex electric fields in the X and Y polarizations. The Stokes parameters of the field S_0, S_1, S_2, S_3, and the Stokes vector $\mathbf{S} = [S_1, S_2, S_3]^T$ are derived from the Jones vector as

$$\begin{aligned} S_0 &= |E_1|^2 + |E_2|^2 \\ &= E_{1,I}^2 + E_{1,Q}^2 + E_{2,I}^2 + E_{2,Q}^2, \\ S_1 &= |E_1|^2 - |E_2|^2 \\ &= E_{1,I}^2 + E_{1,Q}^2 - E_{2,I}^2 - E_{2,Q}^2, \\ S_2 &= 2\mathrm{Re}\{E_1 E_2^*\} \\ &= 2E_{1,I}E_{2,I} + 2E_{1,Q}E_{2,Q}, \\ S_3 &= 2\mathrm{Im}\{E_1 E_2^*\} \\ &= -2E_{1,I}E_{2,Q} + 2E_{1,Q}E_{2,I}. \end{aligned} \tag{1}$$

Note that our definition of $\mathbf{S}$ does not include the zeroth Stokes parameter S_0 since it does not contain additional information, i.e., $S_0 = \sqrt{S_1^2 + S_2^2 + S_3^2} = \|\mathbf{S}\|_2$.

SV detection extracts information from a received optical signal by detecting information that has been modulated in $\mathbf{S}$. Fig. 1(a) depicts an exemplary SV detection system. An input message sequence is mapped to symbols, which are converted to drive voltage signals V_1, V_2, and V_3 that modulate $\mathbf{S}$ onto a sequence of minimum-bandwidth pulses in the optical electric field. Several SV modulator designs have been proposed, such as the dual-polarization in-phase quadrature modulator (DPIQM) shown in Fig. 1(b) and the Kikuchi modulator (KM) [6] shown in Fig. 1(c). Note that, while a standard DPIQM has four amplitude modulators, we can remove one without loss of generality for SV detection [18]. Both modulator designs require three input drive voltages and can modulate any arbitrary $\mathbf{S}$; Section VI-A discusses the drive level requirements of both in greater detail.

In Fig. 1(a), the modulated optical electric field is coupled into SMF, occupying a bandwidth B around the carrier frequency. The link contains an optical amplifier (OA) before the SV receiver, which optically amplifies the signal while adding complex ASE. This ASE has one-sided power spectral density (PSD) S_{ASE} in each polarization, which is filtered to a bandwidth B by a subsequent optical band-pass filter (BPF) centered around the carrier frequency.

The SV receiver in Fig. 1(d) beats the received signal against itself to generate electrical outputs corresponding to the SV of the received electric field $\check{\boldsymbol{S}} = [\check{S}_1, \check{S}_2, \check{S}_3]$. These electrical outputs are subsequently passed through low-pass filters with cutoff frequency B, then sampled at the symbol rate. While many SV receiver architectures exist, this one is convenient to analyze because it includes a minimum number of electrical outputs, each one directly proportional to a SV component, and all outputs have similar noise characteristics [27].

In Fig. 1(a), the sampled electrical outputs are input to a memoryless equalizer which compensates polarization rotation and linear fiber effects. We assume the equalizer has perfect knowledge of the channel, which can be obtained in practice with blind channel estimation [27]. Lastly, a detector maps the equalized signal to symbols and then messages.

Under the monochromatic signal approximation [28, ch. 7], at the output photodiodes, the dominant signal-spontaneous beat noise has one-sided PSD $4R^2 P_{\text{in}} \frac{S_{\text{ASE}}}{2}$ uniform over the frequency band $[0, B/2]$, where P_{in} is the received optical power and R is the photodiode responsivity. After passing through the low-pass filters, the signal-spontaneous beat noise has total power $4R^2 P_{\text{in}} \frac{S_{\text{ASE}}}{2} \frac{B}{2}$. If we assume an input discrete-time optical signal with power P_{in} and variance σ^2_{amp} in each real dimension,

equating the continuous-time and discrete-time models gives $\sigma^2_{\text{amp}} = \frac{1}{4} S_{\text{ASE}} B$ [16].

For simplicity, this model neglects distortion from polarization mode dispersion, polarization-dependent loss, Kerr nonlinearity, and chromatic dispersion. Chromatic dispersion is a significant hindrance to longer-reach SV detection systems; optical dispersion compensation could be employed to mitigate its impact, as in [18].

B. Channel Model

We now present a model for the ASVD channel in Fig. 1(a). The SMF and OA correspond to a Jones matrix $\mathbf{U}$, which is a scaled unitary matrix such that $\mathbf{U}^H\mathbf{U} = \sqrt{\varsigma}\mathbf{I}_2$, where ς is the channel gain factor and $\mathbf{I}_2$ is the 2×2 identity matrix. Complementarily, the SMF and OA also correspond to a Mueller matrix $\mathbf{H}$, where $\mathbf{H}$ is a scaled orthogonal matrix with $\mathbf{H}^T\mathbf{H} = \varsigma\mathbf{I}_3$ [29]. At the input of the SV receiver, the Jones vector of the ASE noise can be written as

$$\boldsymbol{N} = [N_1, N_2] = [N_{1I} + jN_{1Q}, N_{2I} + jN_{2Q}], \tag{2}$$

with covariance matrix $2\sigma^2_{\text{amp}}\mathbf{I}_2$. This is complex circularly symmetric additive white Gaussian noise (AWGN) with variance $2\sigma^2_{\text{amp}}$ in each complex dimension.

Let $\mathbf{E}$ denote the transmitted Jones vector and $\mathbf{S}$ denote the corresponding SV. The Jones and Stokes vectors before reception, $\check{\boldsymbol{E}}$ and $\check{\boldsymbol{S}}$ respectively, are random vectors given by

$$\check{\boldsymbol{E}} = \mathbf{U}\mathbf{E} + \boldsymbol{N} = \mathbf{E}' + \boldsymbol{N}, \tag{3}$$

$$\check{\boldsymbol{S}} = \mathbf{H}\mathbf{S} + \check{\boldsymbol{N}} = \mathbf{S}' + \check{\boldsymbol{N}}, \tag{4}$$

where $\mathbf{E}'$ and $\mathbf{S}'$ are the noiseless Jones and Stokes vectors after transformation by $\mathbf{U}$ and $\mathbf{H}$ respectively and $\check{\boldsymbol{N}} = [\check{N}_1, \check{N}_2, \check{N}_3]$ is a random vector of spontaneous-spontaneous and signal-spontaneous beat noises. The values of $\check{\boldsymbol{S}}$ and $\check{\boldsymbol{N}}$ can be derived from (1) and (2):

$$\begin{aligned}
\check{S}_1 &= (E'_{1I} + N_{1I})^2 + (E'_{1Q} + N_{1Q})^2 \\
&\quad - (E'_{2I} + N_{2I})^2 - (E'_{2Q} + N_{2Q})^2, \\
\check{S}_2 &= 2(E'_{1I} + N_{1I})(E'_{2I} + N_{2I}) \\
&\quad - 2(E'_{1Q} + N_{1Q})(E'_{2Q} + N_{2Q}), \\
\check{S}_3 &= -2(E'_{1I} + N_{1I})(E'_{2Q} + N_{2Q}) \\
&\quad + 2(E'_{1Q} + N_{1Q})(E'_{2I} + N_{2I}),
\end{aligned} \tag{5}$$

$$\begin{aligned}
\check{N}_1 &= 2N_{1I}E'_{1I} + 2N_{1Q}E'_{1Q} - 2N_{2I}E'_{2I} - 2N_{2Q}E'_{2Q} \\
&\quad + N^2_{1I} + N^2_{1Q} - N^2_{2I} - N^2_{2Q}, \\
\check{N}_2 &= 2N_{1I}E'_{2I} + 2N_{1Q}E'_{2Q} + 2N_{2I}E'_{1I} + 2N_{2Q}E'_{1Q} \\
&\quad + 2N_{1I}N_{2I} + 2N_{1Q}N_{2Q}, \\
\check{N}_3 &= -2N_{1I}E'_{2Q} + 2N_{1Q}E'_{2I} + 2N_{2I}E'_{1Q} - 2N_{2Q}E'_{1I} \\
&\quad - 2N_{1I}N_{2Q} + 2N_{1Q}N_{2I}.
\end{aligned} \tag{6}$$

Each $\check{N}_i$ can be expressed as the sum of the squares of independent Gaussian random variables; thus, they follow generalized chi-squared distributions, differing in their non-centrality and offset parameters. Note that the exact noise distributions of $\check{N}_1, \check{N}_2$, and $\check{N}_3$ are mutually correlated and we have not been able to find an analytical formula for their mutual distribution. However, at high signal-to-noise ratios (SNRs), $\check{\boldsymbol{N}}$ is dominated by the signal-spontaneous beat terms. Thus, we can form a vector of approximate noise variables that neglects the spontaneous-spontaneous beat terms, $\widetilde{\boldsymbol{N}} = [\widetilde{N}_1, \widetilde{N}_2, \widetilde{N}_3] \approx \check{\boldsymbol{N}}$, where each $\widetilde{N}_i$ is the sum of four uncorrelated zero-mean Gaussian random variables:

$$\begin{aligned}
\widetilde{N}_1 &= 2N_{1I}E'_{1I} + 2N_{1Q}E'_{1Q} - 2N_{2I}E'_{2I} - 2N_{2Q}E'_{2Q}, \\
\widetilde{N}_2 &= 2N_{1I}E'_{2I} + 2N_{1Q}E'_{2Q} + 2N_{2I}E'_{1I} + 2N_{2Q}E'_{1Q}, \\
\widetilde{N}_3 &= -2N_{1I}E'_{2Q} + 2N_{1Q}E'_{2I} + 2N_{2I}E'_{1Q} - 2N_{2Q}E'_{1I}.
\end{aligned} \tag{7}$$

The three noise variables $\widetilde{N}_1, \widetilde{N}_2$, and $\widetilde{N}_3$ are uncorrelated conditioned on a fixed S_0 [30]. Noting that $\|\mathbf{S}\|_2 = E^2_{1I} + E^2_{1Q} + E^2_{2I} + E^2_{2Q}$, the covariance of $\widetilde{\boldsymbol{N}}$ can be derived as $\text{cov}(\widetilde{\boldsymbol{N}}) = 4\sigma^2_{\text{amp}}\|\mathbf{E}'\|^2_2\mathbf{I}_3 = 4\sigma^2_{\text{amp}}\sqrt{\varsigma}\|\mathbf{S}\|_2\mathbf{I}_3$ [16]. For tractability, we use the approximate noise distribution of $\widetilde{\boldsymbol{N}}$ for further derivations, but still use the exact noise model for $\check{\boldsymbol{N}}$ to evaluate constellation performance in Section V.

The output of the equalizer is found by applying $\mathbf{H}^T$ onto $\check{\boldsymbol{S}}$ and is given by $\boldsymbol{S}_{\text{eq}} = \frac{1}{\varsigma}\mathbf{H}^T\check{\boldsymbol{S}} \approx \mathbf{S} + \frac{1}{\varsigma}\mathbf{H}^T\widetilde{\boldsymbol{N}}$, where

$$\text{cov}\left(\frac{1}{\varsigma}\mathbf{H}^T\widetilde{\boldsymbol{N}}\right) = 4\frac{\sigma^2_{\text{amp}}\|\mathbf{S}\|_2}{\sqrt{\varsigma}}\mathbf{I}_3. \tag{8}$$

In other words, the equalized signal has noise which is approximately distributed as a three-dimensional, spherically symmetric Gaussian, with variance scaled by the transmitted optical power $\|\mathbf{S}\|_2$; we denote this as signal-dependent noise. Finally, we can write an approximate channel model with signal-dependent noise $\boldsymbol{N}_{\text{eq}}$ for the equalized SV as

$$\begin{gathered}
\boldsymbol{S}_{\text{eq}} \approx \mathbf{S} + \boldsymbol{N}_{\text{eq}} \\
\text{where } \boldsymbol{N}_{\text{eq}} \sim \mathcal{N}_3\left(\mu = 0, \Sigma = 4\tfrac{\sigma^2_{\text{amp}}\|\mathbf{S}\|_2}{\sqrt{\varsigma}}\mathbf{I}_3\right).
\end{gathered} \tag{9}$$

III. Constellation Design Preliminaries

In this section, we derive an objective function for optimizing ASVD constellations. Section III-A introduces notation for our detection scheme and error probabilities. Section III-B specifies a decision statistic, then derives approximate pairwise error probabilities and a union bound SER for ASVD constellations. Section III-C derives an objective function for constellation optimization from the union bound SER. Section III-D provides a geometric understanding of the objective function as a scaled-sphere packing problem.

A. Detection and Error Probability Terminology

A constellation $\mathcal{C}$ is a set of M symbols $\{\mathbf{X}_1, \mathbf{X}_2, \ldots, \mathbf{X}_M\}$ that map to messages $\{1, 2, \ldots, M\}$ [31, ch. 4]. To decide which message was transmitted, for each message i the detector defines a decision statistic $\text{Z}_i(\mathbf{S}_{\text{eq}})$ which is a function of the observation

$\mathbf{S}_{\text{eq}}$ taken of the random vector $\boldsymbol{S}_{\text{eq}}$. The detected message $\widehat{i}$ is the message corresponding to the largest decision statistic, or

$$\widehat{i} = \underset{i\in[1,M]}{\arg\max}\ \mathrm{Z}_i(\mathbf{S}_{\text{eq}}). \tag{10}$$

Equivalently, (10) partitions the reception space into M disjoint decision regions $\{\Gamma_1, \Gamma_2, \ldots, \Gamma_M\}$. Γ_i is the volume in the observation space of $\boldsymbol{S}_{\text{eq}}$ such that if the observed $\mathbf{S}_{\text{eq}}$ is within Γ_i, then the detected message is i, or analytically,

$$\Gamma_i = \{\mathbf{S}_{\text{eq}} \mid \mathrm{Z}_i(\mathbf{S}_{\text{eq}}) > \mathrm{Z}_j(\mathbf{S}_{\text{eq}})\, \forall j \neq i\}. \tag{11}$$

When $\mathbf{X}_i$ is transmitted, a symbol error occurs when $\mathbf{S}_{\text{eq}}$ is not within Γ_i; thus, the symbol-error probability $P_{\text{e}|i}$ is

$$P_{\text{e}|i} = \mathrm{P}(\mathbf{S}_{\text{eq}} \notin \Gamma_i \mid \mathbf{S} = \mathbf{X}_i). \tag{12}$$

The SER for a constellation, P_{e}, is the average symbol-error probability over all messages. In this paper, we consider constellations with equiprobable messages, where

$$P_{\text{e}} = \frac{1}{M}\sum_{i=1}^{M} P_{\text{e}|i}. \tag{13}$$

B. Approximate Error Probabilities

We now derive an approximate union bound for the SER of an ASVD constellation. To do so, we must first derive a decision statistic and find an approximate pairwise error probability.

The maximum-likelihood (ML) decision statistic $\mathrm{Z}_i^{\text{ML}}(\mathbf{S}_{\text{eq}})$ is defined as the conditional probability density of $\boldsymbol{S}_{\text{eq}}$ given that message i was transmitted,

$$\mathrm{Z}_i^{\text{ML}}(\mathbf{S}_{\text{eq}}) = f_{\boldsymbol{S}_{\text{eq}}}(\mathbf{S}_{\text{eq}} \mid \mathbf{S} = \mathbf{X}_i), \tag{14}$$

where $f_{\boldsymbol{S}_{\text{eq}}}(\mathbf{S}_{\text{eq}})$ is probability density function of $\boldsymbol{S}_{\text{eq}}$. Since we do not have an analytical formula for the exact noise distribution, we cannot derive the exact ML decision statistics and must instead find an approximation. A straightforward approach is to use the conditional probability density of the approximate noise distribution, which we denote as $\mathrm{Z}_i^{\widetilde{\text{ML}}}(\mathbf{S}_{\text{eq}})$:

$$\mathrm{Z}_i^{\widetilde{\text{ML}}}(\mathbf{S}_{\text{eq}}) = f_{\boldsymbol{N}_{\text{eq}}}(\mathbf{S}_{\text{eq}} - \mathbf{S} \mid \mathbf{S} = \mathbf{X}_i). \tag{15}$$

Another approximate decision statistic arises when deriving a planar decision boundary that gives equal-crossover pairwise error probability. The pairwise error probability $P_{i|j}$ is the probability that the detector favors message i over j given that j is transmitted:

$$P_{i|j} = \mathrm{P}(\mathrm{Z}_i(\mathbf{S}_{\text{eq}}) > \mathrm{Z}_j(\mathbf{S}_{\text{eq}}) \mid \mathbf{S} = \mathbf{X}_j). \tag{16}$$

Given these two messages, we use the term decision boundary to describe the surface in the observation space of $\boldsymbol{S}_{\text{eq}}$ where their decision statistics are equal:[1]

$$\{\mathbf{S}_{\text{eq}} \mid \mathrm{Z}_i(\mathbf{S}_{\text{eq}}) = \mathrm{Z}_j(\mathbf{S}_{\text{eq}})\}. \tag{17}$$

[1]Strictly speaking, in digital communications a decision boundary refers to the surface in the observation space that lies between two decision regions Γ_i and Γ_j. We use a more general definition to allow us to characterize the boundary when considering only the messages $\{i, j\}$, instead of the entire set of possible messages $\{1, 2, \ldots, M\}$.

Using the approximate noise distribution, the planar decision boundary that gives minimal equal-crossover pairwise error probability is the plane perpendicular to $\mathbf{X}_i - \mathbf{X}_j$ passing through the point μ,

$$\mu = \frac{\mathbf{X}_i\sqrt{\|\mathbf{X}_j\|_2} + \mathbf{X}_j\sqrt{\|\mathbf{X}_i\|_2}}{\sqrt{\|\mathbf{X}_i\|_2} + \sqrt{\|\mathbf{X}_j\|_2}}. \tag{18}$$

Integrating the approximate noise distribution across this planar boundary gives the following approximation for the pairwise error probability:

$$P_{i|j} \approx \mathrm{Q}\left(\frac{\|\mathbf{X}_j - \mu\|_2}{\frac{2\sigma_{\text{amp}}}{\sqrt[4]{\varsigma}}\sqrt{\|\mathbf{X}_j\|_2}}\right) = \mathrm{Q}\left(\sqrt{\frac{\sqrt{\varsigma}\,\mathrm{d}(\mathbf{X}_i, \mathbf{X}_j)^2}{4\sigma_{\text{amp}}^2}}\right), \tag{19}$$

$$\mathrm{d}(\mathbf{X}_i, \mathbf{X}_j) = \frac{\|\mathbf{X}_i - \mathbf{X}_j\|_2}{(\sqrt{\|\mathbf{X}_i\|_2} + \sqrt{\|\mathbf{X}_j\|_2})}, \tag{20}$$

where Q is the tail distribution of the standard normal distribution [16]. $\mathrm{d}(\mathbf{X}_i, \mathbf{X}_j)$ is a distance function in the observation space of $\boldsymbol{S}_{\text{eq}}$ which determines the pairwise error probability between two symbols. We can consider a decision statistic $\mathrm{Z}_i^{\mathrm{d}}(\mathbf{S}_{\text{eq}})$ that measures the distance d between $\mathbf{S}_{\text{eq}}$ and the symbol $\mathbf{X}_i$, analytically given by

$$\mathrm{Z}_i^{\mathrm{d}}(\mathbf{S}_{\text{eq}}) = -\mathrm{d}(\mathbf{S}_{\text{eq}}, \mathbf{X}_i). \tag{21}$$

In simulations, we find that using $\mathrm{Z}_i^{\mathrm{d}}(\mathbf{S}_{\text{eq}})$ results in better receiver sensitivity than $\mathrm{Z}_i^{\widetilde{\text{ML}}}(\mathbf{S}_{\text{eq}})$ when using exact noise models and thus we use $\mathrm{Z}_i^{\mathrm{d}}(\mathbf{S}_{\text{eq}})$ for approximation of error probabilities.

In the observation space, $\mathrm{Z}_i^{\mathrm{d}}(\mathbf{S}_{\text{eq}})$ forms a decision boundary between two messages that is a quadric surface containing μ. At high SNR, pairwise errors are most likely to occur near μ due to the exponential decay of the approximate noise distribution. Thus, we can approximate the decision boundary as the plane tangent to the quadric surface at μ. This plane is identical to the planar boundary used in (19); thus, (19) also approximates the pairwise error probability when using $\mathrm{Z}_i^{\mathrm{d}}(\mathbf{S}_{\text{eq}})$.

To estimate the overall constellation SER, we take the sum of the approximate pairwise error probabilities between all symbols, which is known as a union bound. The union bound SER, which we denote as $\widetilde{P}_{\text{e}}$, can be written as

$$\widetilde{P}_{\text{e}} \approx \frac{1}{M}\sum_{i=1}^{M}\sum_{\substack{j=1\\ j\neq i}}^{M} \mathrm{Q}\left(\sqrt{\frac{\sqrt{\varsigma}\,\mathrm{d}(\mathbf{X}_i, \mathbf{X}_j)^2}{4\sigma_{\text{amp}}^2}}\right). \tag{22}$$

Since we neglect noise sources and can double count errors, the union bound is not an upper or lower bound on the SER, but still approximates it well at high SNR.

C. Constellation Design Objective

In the limit of high SNR, $\widetilde{P}_{\text{e}}$ is dominated by pairs of symbols with minimal $\mathrm{d}(\mathbf{X}_i, \mathbf{X}_j)$. Thus, similar to [19], [24], we can express $\widetilde{P}_{\text{e}}$ as approximately proportional to an asymptotic power

efficiency γ and the average transmitted optical power P:

$$\widetilde{P}_{\mathrm{e}} \,\widetilde{\propto}\, \mathrm{Q}\left(\sqrt{\frac{\gamma P\sqrt{\varsigma}}{2\sigma_{\mathrm{amp}}^2 \log_2 M}}\right), \tag{23}$$

$$\gamma = \frac{\log_2 M}{2P} \min_{\mathbf{X}_i,\mathbf{X}_j\in\mathcal{C},i\neq j} \mathrm{d}(\mathbf{X}_i,\mathbf{X}_j)^2, \tag{24}$$

$$P = \frac{1}{M}\sum_{\mathbf{X}_i\in\mathcal{C}} \|\mathbf{X}_i\|_2 . \tag{25}$$

γ is inversely proportional to the P needed to achieve a given SER and thus represents the constellation's influence on the receiver sensitivity [32, p. 220]. We can find a power-efficient constellation $\mathcal{C}_{\mathrm{opt}}$ for a fixed M by maximizing γ, i.e., using the objective function

$$\mathcal{C}_{\mathrm{opt}} = \underset{\mathcal{C}\subset\mathbb{R}^3,|\mathcal{C}|=M}{\arg\max} \left(\frac{\min_{\mathbf{X}_i,\mathbf{X}_j\in\mathcal{C},i\neq j} \mathrm{d}(\mathbf{X}_i,\mathbf{X}_j)^2}{\sum_{\mathbf{X}_i\in\mathcal{C}} \|\mathbf{X}_i\|_2}\right), \tag{26}$$

where we have combined (24) and (25) and simplified out constants. To simplify (26), note that γ is constant with respect to P, and thus finding a solution where $\min \mathrm{d}(\mathbf{X}_i,\mathbf{X}_j)^2 = 1$ still results in an optimal solution. So, $\mathcal{C}_{\mathrm{opt}}$ can instead be found using

$$\begin{aligned}\mathcal{C}_{\mathrm{opt}} = \underset{\mathcal{C}\subset\mathbb{R}^3,|\mathcal{C}|=M}{\arg\min} &\left(\sum_{\mathbf{X}_i\in\mathcal{C}} \|\mathbf{X}_i\|_2\right) \\ \text{subject to } \mathrm{d}(\mathbf{X}_i,\mathbf{X}_j)^2 \geq 1 \;\; &\forall \mathbf{X}_i,\mathbf{X}_j \in \mathcal{C}_{\mathrm{opt}}, i\neq j.\end{aligned} \tag{27}$$

D. Scaled-Sphere Packing

From (27), we can form a more intuitive, geometric approach to optimizing ASVD constellations. First, the constraint can be rewritten as $\|\mathbf{X}_i-\mathbf{X}_j\|_2 - \sqrt{\|\mathbf{X}_i\|_2} - \sqrt{\|\mathbf{X}_j\|_2} \geq 0$. From this constraint, each $\mathbf{X}_i$ can be thought of as a sphere with radius equal to the square root of the ℓ^2-norm of its center, $r_i = \sqrt{\|\mathbf{X}_i\|_2}$; we denote this as a scaled sphere. Then, the objective function simply minimizes the average ℓ^2-norm of the scaled spheres' centers while ensuring that no scaled spheres overlap. We refer to this problem as *scaled-sphere packing*; by (27), finding a dense scaled-sphere packing is equivalent to designing a power-efficient ASVD constellation.

To the best of our knowledge, the scaled-sphere packing problem has not been studied previously. Additionally, it is more challenging to solve than the more common equiradial sphere packing problem, due to the lack of translational symmetry and variable sphere sizes. We focus on numerically generated solutions since, even for equiradial sphere packings, analytical solutions can be difficult to find [33, ch. 1].

IV. Constellation Design Methods

A. Optimized Design

Reference [34] presents a method to create minimal-energy clusters of hard, equiradial spheres, which leads to optimal packings for up to thirty-two spheres in up to four dimensions. It reformulates a minimal-energy objective to incorporate two parameters α and β, respectively representing the hardness and repulsion of the spheres. Then, it successively optimizes the packing under a sequence of these objectives, with each iteration of the objective making the spheres harder and less repulsive.

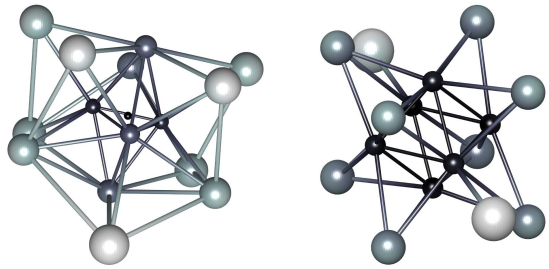

(a) Optimized Constellation (b) Practical Constellation

Fig. 2. 16-ary ASVD constellations with connections drawn between all symbols with minimal $\mathrm{d}(\mathbf{X}_i,\mathbf{X}_j)$. Darker symbols and connections are closer to the origin.

Rewriting the objective from [34] to optimize an ASVD constellation, minimizing the average optical power of SV symbols, gives

$$\begin{aligned}\Phi(\mathcal{C}_k) &= \sum_{i=1}^{M}\left(\|\mathbf{X}_i\|_2 + \textstyle\sum_{\substack{j=1\\ j\neq i}}^{M} \frac{\beta_k}{\mathrm{d}(\mathbf{X}_i,\mathbf{X}_j)-\alpha_k}\right), \\ \alpha_{k+1} &= \alpha_k + \min_{\mathbf{X}_i,\mathbf{X}_j\in\mathcal{C}_k,i\neq j} \frac{\mathrm{d}(\mathbf{X}_i,\mathbf{X}_j)-\alpha_k}{2}, \\ \beta_{k+1} &= 0.5\beta_k.\end{aligned} \tag{28}$$

We initialize the optimization with soft scaled spheres that strongly repulse each other ($\alpha_0 = 0$ and $\beta_0 = 1$) and a random $\mathcal{C}_0$, then optimize the objective function $\Phi(\mathcal{C}_0)$ until convergence. We iterate α and β, re-optimize $\mathcal{C}$, and then repeat iterations until convergence. We repeat the optimization for several random initializations and take the resulting $\mathcal{C}$ with the largest γ as the output constellation. Due to the non-convexity of the problem, we use gradient descent as our optimizer, minimizing $\Phi(\mathcal{C}_k)$ at each iteration. To reproduce the methodology from [34], once optimal constellations are determined, we obtain additional constellations by taking a random symbol and placing it outside the constellation, then reinitializing the optimization with $\alpha_0 = 0.9\cdot\min(\mathrm{d}(\mathbf{X}_i,\mathbf{X}_j))$ and a random $\beta_0 \in (0,1]$. We denote constellations designed using this method as *optimized constellations*.

Within the resulting optimized constellations, there are some recognizable structures.

- All constellations have a symbol at the origin.
- The 2-ary optimized constellation is on-off keying.
- The 4-ary optimized constellation has the non-zero symbols equally spaced around the origin, forming an equilateral triangle.
- The 16-ary constellation has one plane of reflection symmetry (Fig. 2(a)).

However, several features of the optimized constellations are not conducive to implementation in short reach optical communications systems:

- The symbol at the origin breaks the assumption of high SNR used in (9), and thus its output distribution does not match the approximate noise distribution.
- Each respective $\mathbf{X}_i$ has mostly distinct values of the Stokes parameters S_1, S_2, and S_3. This means the modulator

TABLE I
SYMBOL EQUIVALENCE CLASSES, EACH LISTING A REPRESENTATIVE SYMBOL, THE NUMBER OF IMPLIED SYMBOLS TO ENSURE $\mathbf{O_h}$ SYMMETRY, AND THE POLYHEDRON FORMED BY THE SYMBOLS IN THE CLASS. FOR EACH REPRESENTATIVE SYMBOL, $a \neq B \neq C \neq 0$.

Representative Symbol	Symbols in Class	Uniform $\mathbf{O_h}$-symmetric Polyhedron
$(a, 0, 0)$	6	Octahedron
(a, a, a)	8	Cube
$(a, a, 0)$	12	Cuboctahedron
$(a, b, 0)$	24	Truncated octahedron
(a, b, b)	24	Truncated cube or rhombicuboctahedron
(a, b, c)	48	Truncated cuboctahedron

requires many unequally spaced, unique drive levels to modulate the constellations.
- The lack of symmetry decreases redundancy when implementing decision regions, requiring more complex hardware at the detector.

To address these concerns, we propose a second method of designing constellations which results in constellations with slightly inferior sensitivities, but less stringent implementation constraints compared to the optimized constellations.

B. Practical Design

To improve the practicality of ASVD constellations, we constrain the constellation symbols to have full octahedral symmetry, which we shorthand as $\mathbf{O_h}$ symmetry [35, pp. 243–245]. We decide on this constraint because:
- Enforcing symmetry reduces the hardware complexity for modulating and detecting a constellation, since modulator levels and decision regions will also have symmetry.
- Subsets of primitive square and cubic lattice cosets are some of the most common constellations in communications [36] and the three-dimensional cubic lattice has both translational symmetry and $\mathbf{O_h}$ symmetry [37].
- Due to the signal-dependent noise, enforcing translational symmetry causes significant degradation in receiver sensitivity for larger ASVD constellations ($M > 8$).
- On the other hand, requiring $\mathbf{O_h}$ symmetry causes much less degradation in receiver sensitivity, since the variance of the signal-dependent noise remains constant under rotation about the origin.

To reduce the total number of symbols in the constellation to M, we allow the highest power shell of symbols to be a subset of an originally $\mathbf{O_h}$-symmetric shell, similar to [18]. Additionally, we do not include a symbol at the origin due to the difficulties mentioned in Section IV-A.

We can define six equivalence classes of symbols as shown in Table I, where a class consists of all symbols that have $\mathbf{O_h}$ symmetry with a representative symbol. To visualize this, it may be helpful to note that classes of symbols form the vertices of different uniform $\mathbf{O_h}$-symmetric polyhedra. Each symbol will fix the placement of all other symbols in its class and it is not trivial to move symbols between classes; since the optimization-based method from Section IV-A requires symbols to move freely, it cannot be repurposed for this new problem. Instead, we turn to a different packing strategy from [34], a *greedy* algorithm where equiradial spheres are placed sequentially to minimize the energy added at each step. This algorithm does not result in an optimal packing for equiradial spheres for most values of M; however, by sequentially placing shells of $\mathbf{O_h}$-symmetric symbol classes, we ensure the resulting constellation is $\mathbf{O_h}$-symmetric. Since enforcing the $\mathbf{O_h}$ symmetry significantly reduces the number of possible solutions, we can perform an exhaustive search of all possible greedy $\mathbf{O_h}$-symmetric constellations. The detailed process is:
1) Determine all possible permutations of the equivalence classes such that the total number of symbols is M or exceeds M by the final class of symbols.
2) For each permutation of classes, sequentially place the classes of symbols such that each shell has minimal power and none of the scaled spheres overlap.
3) If the outermost shell causes the constellation to exceed M symbols, cull excess symbols from that shell to maximize the distance between the remaining symbols.
4) Compare all the constellations generated by the permutations, and designate the one with the lowest average power as the chosen constellation.

Fig. 3 shows the greedy stepwise placement of shells for the 64-ary $\mathbf{O_h}$-symmetric constellation. We denote constellations designed using this method as *practical constellations*.

The structures of some of the practical constellations with lower modulation orders are as follows:
- The 2-ary practical constellation is binary phase-shift keying (identical to the 2-ary constellation from [6]).
- The 4-ary practical constellation is the three-dimensional simplex, a tetrahedron (also identical to the 4-ary constellation from [6]).
- The 8-ary practical constellation is not a cube, as might be expected. Instead, it has two shells: an interior octahedron and a culled exterior cube.

As seen in the 16-ary practical constellation in Fig. 2(b), the practical constellations are more regularly spaced and symmetric than the optimized constellations, and thus more easily implementable. Furthermore, in Section V, we will show that the performance of practical constellations is close to that of optimal constellations, especially for higher modulation orders.

V. CONSTELLATION DESIGNS AND PERFORMANCE

We compare our optimized and practical constellations with those proposed by Kikuchi and Kawakami [6], which are subsets of primitive cubic lattice cosets for $M = 2, 4, 8$, and 64, and cubic shells for $M = 16$ and 32, and those proposed by Morsy-Osman et al. [18], which are subsets of face-centered cubic (FCC) lattices with no symbol at the origin for $M = 16$ and 64. Although the constellations in [18] were designed assuming the TSVD noise model, they theoretically perform better than the constellations proposed by [6] and were evaluated in a system including an optical amplifier. For practicality, we only design constellations where M is a power of two. Since the 2-ary and

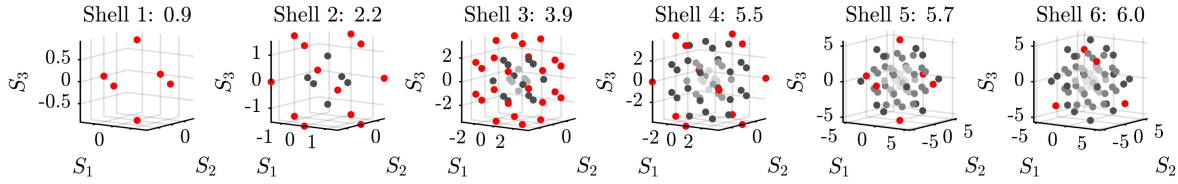

Fig. 3. Greedy formation of the 64-ary practical constellation. From left to right, $\mathbf{O_h}$-symmetric shells are layered successively with increasing radii such that the scaled spheres about each symbol do not intersect. New symbols are shown in red, older symbols become increasingly lighter, and each shell is labeled with its distance from the origin. For $M = 64$, the optimal symbol class permutation is (octahedron, cuboctahedron, rhombicuboctahedron, cuboctahedron, octahedron, cube), with half of the symbols culled from the final shell.

TABLE II
CHARACTERISTICS OF EXISTING AND NEWLY DESIGNED ASVD CONSTELLATIONS. CFM: CONSTELLATION FIGURE OF MERIT, PAR: PEAK TO AVERAGE POWER RATIO, FCC: FACE-CENTERED CUBIC.

Modulation Order M	Constellation Type	Asymptotic Efficiency γ (dB)	CFM (dB)	PAR
2	Optimized	−6.01	1.76	2
	Cubic lattice	−9.03	−1.25	1
4	Optimized	−6.01	−1.25	1.33
	Cubic lattice	−7.78	−3.01	1
8	Optimized	−6.93	−3.92	1.85
	Practical	−8.33	−5.32	1.65
	Cubic lattice	−9.03	−6.02	1
16	Optimized	−7.76	−5.99	1.62
	Practical	−8.56	−6.79	1.63
	FCC lattice	−10.24	−8.48	1.28
	Cubic Shells	−10.79	−9.03	1.5
32	Optimized	−8.99	−8.20	1.55
	Practical	−9.34	−8.55	1.41
	Cubic shells	−14.82	−14.02	1.85
64	Optimized	−10.28	−10.28	1.60
	Practical	−10.55	−10.55	1.54
	FCC lattice	−12.81	−12.81	1.32
	Cubic lattice	−13.77	−13.77	1.39

4-ary practical constellations are identical to those designed in [6], we exclude them from our results.

Table II lists the theoretical characteristics of the optimized, practical, FCC, and cubic constellations. The asymptotic power efficiency γ can be used to compare constellations operating at the same bit rate and is defined in (24). The constellation figure of merit (CFM) can be used to compare constellations operating at the same symbol rate and is defined per [36] as

$$\text{CFM} = \frac{6\gamma}{\log_2 M}. \tag{29}$$

Lastly, the peak-to-average power ratio (PAR) is an approximate measure of the challenges a constellation would pose for DACs and modulator drivers, and is defined as

$$\text{PAR} = \frac{\max_{\mathbf{X}_i \in \mathcal{C}} \|\mathbf{X}_i\|_2}{\sum_{\mathbf{X}_i \in \mathcal{C}} \|\mathbf{X}_i\|_2 / M}. \tag{30}$$

To numerically evaluate the SERs of the constellations, we first choose decision statistics that best approximate $\mathrm{Z}_i^{\mathrm{ML}}(\mathbf{S}_{\mathrm{eq}})$, i.e., the decision statistics that result in the best receiver sensitivity. Comparing $\mathrm{Z}_i^{\widetilde{\mathrm{ML}}}(\mathbf{S}_{\mathrm{eq}})$, $\mathrm{Z}_i^{\mathrm{d}}(\mathbf{S}_{\mathrm{eq}})$, and numerically estimated conditional probability distributions, we find that $\mathrm{Z}_i^{\mathrm{d}}(\mathbf{S}_{\mathrm{eq}})$ performs best. Since the approximation of signal-dependent noise no longer applies for a symbol $\mathbf{X}_i$ at the origin, we instead use a scaled Euclidean distance for the decision statistic of that message, i.e., $\mathrm{Z}_i(\mathbf{S}_{\mathrm{eq}}) = -c\|\mathbf{S}_{\mathrm{eq}}\|_2$. We vary the scaling factor c to find the decision statistic that results in the lowest SER at each optical signal-to-noise ratio per bit ($\mathrm{OSNR_b}$), which is defined per [16] as

$$\frac{P\sqrt{\varsigma}}{2\sigma_{\mathrm{amp}}^2 \log_2 M}. \tag{31}$$

Once the decision statistics are determined, we generate realizations of $\boldsymbol{S}_{\mathrm{eq}}$ at different $\mathrm{OSNR_b}$ values using the exact noise models, then estimate the SER. Since the true ML decision statistics are unknown, the SERs calculated in this paper are upper bounds of the constellation performance using ML detection. We note that because most optimized and practical constellations have symbols with more than $\log_2(M)$ nearest neighbors, they cannot be Gray coded; we do not propose a bit-mapping scheme and only evaluate the constellations in terms of their SER.

Fig. 4 shows the SER versus $\mathrm{OSNR_b}$ for different constellation design methods and values of M. The optimized constellations outperform all previously proposed constellations for all values of M. Additionally, the practical constellations improve over all previously proposed constellations for $M \geq 8$, but are still outperformed by the optimized constellations. However, the practical and optimized constellations perform increasingly similarly as M increases, with a receiver sensitivity gap of approximately 0.3 dB at $P_{\mathrm{e}} = 10^{-4}$ for the 32-ary and 64-ary constellations.

Asymptotically, the best-performing constellation at a constant bit rate is the 4-ary optimized constellation. While it has the same asymptotic efficiency as the 2-ary optimized constellation, the symbol at the origin, whose noise is significantly underestimated by the approximate noise model (9), is less likely to be transmitted in the 4-ary constellation. Thus the 4-ary constellation has better receiver sensitivity when evaluated with the exact noise models.

Fig. 5 shows the spectral efficiency (defined as $2/3 \log_2 M$ for SV detection [36]) of different constellations versus the required $\mathrm{OSNR_b}$ to achieve an SER threshold of $P_{\mathrm{e}} = 4.4 \times 10^{-4}$. This threshold corresponds to the KP4 error threshold [38], assuming a symbol error results in, on average, half of the encoded bits being decoded incorrectly. At $M = 2, 4$, and 8 respectively, the

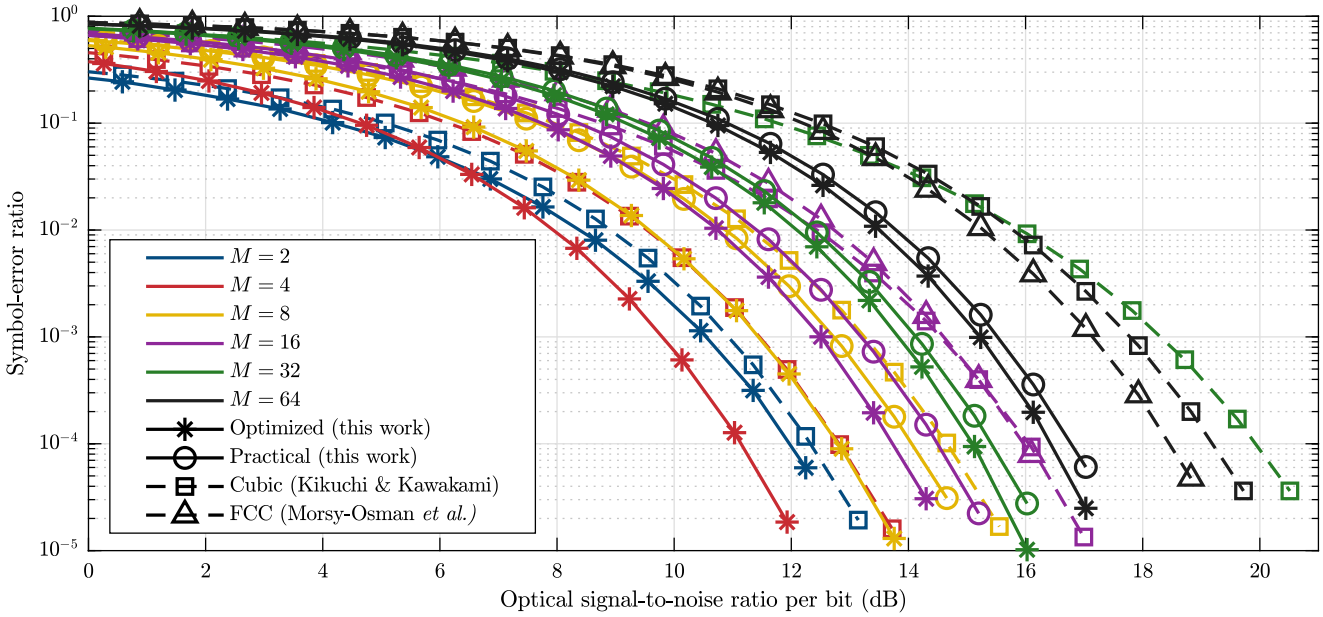

Fig. 4. Symbol-error ratio versus optical signal-to-noise ratio per bit for various constellations. Line colors denote values of M and markers denote constellation design methods. All plotted points represent at least 100 symbol errors in simulation at a given optical signal-to-noise ratio per bit.

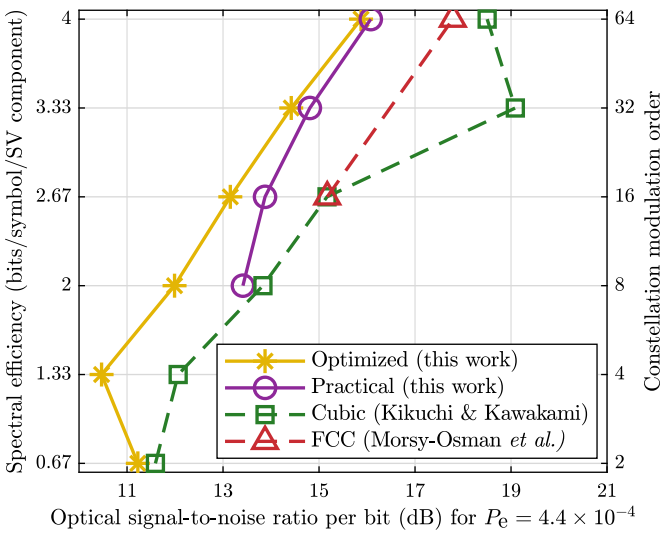

Fig. 5. Spectral efficiency versus optical signal-to-noise ratio per bit required for a symbol-error ratio threshold of 4.4×10^{-4} for various constellations.

optimized constellations have 0.37, 1.63, and 1.84 dB better receiver sensitivity than existing cubic constellations. At $M = 16$ and 64, the optimized constellations improve by 2.02 and 1.91 dB over the existing FCC constellations, while the practical constellations improve by 1.20 and 1.71 dB.

VI. Modulator and Detector Implementation

In the previous sections, our analyses did not consider constraints imposed by physical limitations of the modulator and detector. This section examines the drive voltage levels required by different modulator structures and how simplified decision boundaries and analog-to-digital converter (ADC) resolutions impact detector performance. For a more in-depth analysis of the implementation requirements of previously proposed constellations, see [39].

A. Modulator Implementation

The difficulty in modulating constellations for SV detection arises because no modulator maps electrical outputs directly to the Stokes vector; instead, they map to a corresponding Jones vector. However, because of the nonlinear relationship between Jones and Stokes vectors, even a uniformly spaced lattice of Stokes vectors results in many unevenly spaced Jones vector levels, which require very precise DACs to generate. This precision is difficult to achieve at the high speeds required for short reach communications links.

Many papers investigating SV detection use the DPIQM (shown in Fig. 1(b)) due to its availability and ease of use [9], [18]. The DPIQM maps the drive voltages to each polarization's in-phase and quaternary electric field magnitudes. The notable downside to this architecture is the high DAC precision required for higher-order constellations for SV detection; for example, in [18], the 64-ary FCC constellation could not be implemented due to the required number of drive levels. Examining the components of the Jones vectors for the 64-ary lattice-based constellations shows that the phases and magnitudes of the E_1 and E_2 polarizations assume fewer unique values than the in-phase and quaternary values (Fig. 6). So, we can reduce the number of required drive voltage levels by modulating the electric fields' amplitudes and phases instead of in-phase and quaternary values. For example, the KM, proposed in [6] and shown in Fig. 1(c), maps the drive voltages to S_0, the relative magnitude of E_1 and E_2, and the phase of E_1. Although we do

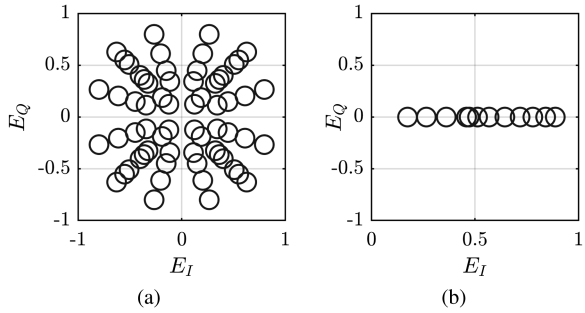

Fig. 6. Possible realization of in-phase E_I and quadrature E_Q Jones vector levels required to modulate a 64-ary cubic constellation in the Stokes space. Plots show (a) the X-polarization E_1 and (b) the Y-polarization E_2. This realization assumes the phase of E_2 is fixed at 0.

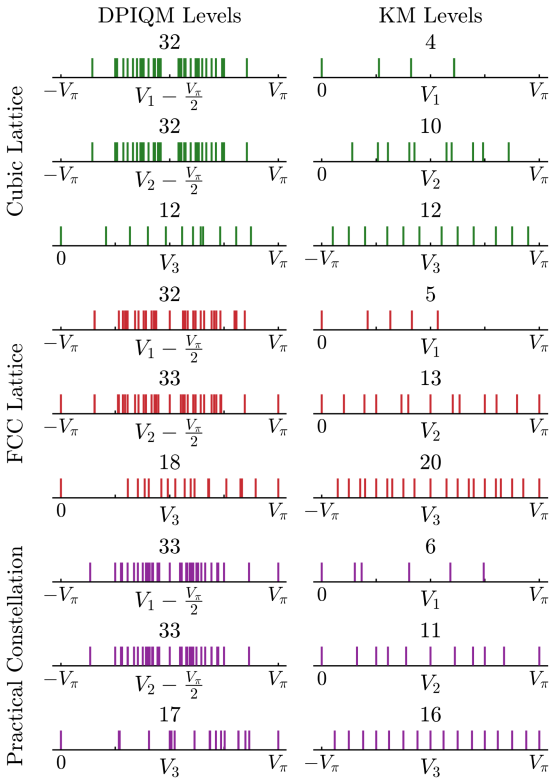

Fig. 7. Required drive voltage levels for the dual-polarization in-phase quadrature modulator (DPIQM) (left column) and Kikuchi modulator (KM) (right column) for the 64-ary cubic constellation, FCC constellation, and practical constellation. These levels assume all amplitude modulators are single-drive Mach-Zehnder interferometers, with a constant bias voltage added to amplitude modulators that require full-swing operation. The numbers above each line are the total number of drive voltage levels for a modulator.

not examine it in detail, the modulator proposed in [8] has drive voltage level requirements comparable to the KM.

Fig. 7 compares the drive voltage levels required to modulate various 64-ary constellations for the DPIQM and the KM. The KM generally has fewer, more uniformly spaced drive voltage levels than the DPIQM. This suggests that the KM can realize modulation of higher-order SV detection constellations more easily than the DPIQM. We also note that the number and spacing of drive voltage levels for the 64-ary practical constellation are similar to those for the 64-ary cubic and FCC constellations.

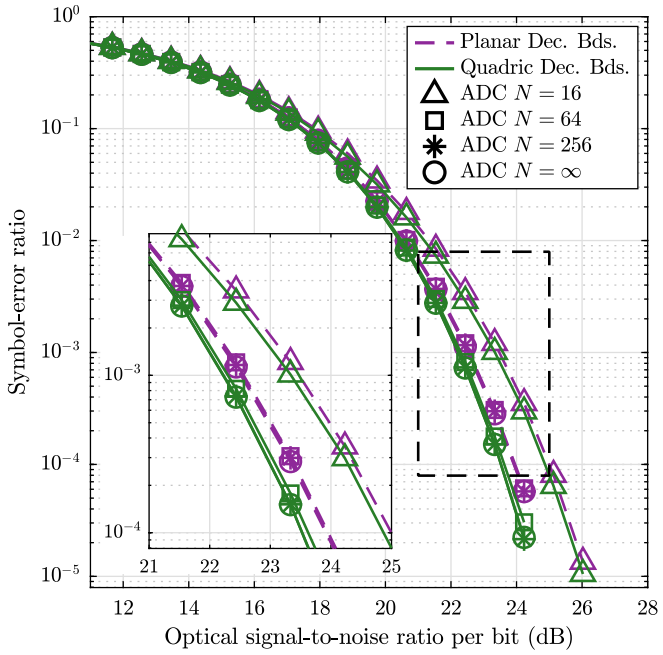

Fig. 8. Receiver sensitivity degradation for a 16-ary practical constellation when considering planar approximations of the $\mathrm{Z}_i^{\mathrm{d}}(\mathbf{S}_{\mathrm{eq}})$ decision boundaries and finite ADC resolution at the receiver. Line color denotes decision boundaries and marker denotes ADC resolution.

This indicates that enforcing $\mathbf{O_h}$ symmetry actually yields more easily implementable constellations.

B. Detector Implementation

In Section V, we evaluate constellations using the $\mathrm{Z}_i^{\mathrm{d}}(\mathbf{S}_{\mathrm{eq}})$ decision statistics to provide close bounds to their optimal performance. As discussed in Section III-B, this forms decision boundaries that are quadric surfaces in the observation space of $\boldsymbol{S}_{\mathrm{eq}}$, which can be challenging to implement at the high speeds required for short reach optical communications systems. Additionally, the simulations in Section V do not consider the effect of finite receiver ADC resolution on the SER, which is important to account for since ASVD constellations have symbols that tend to be nonuniformly distributed in the observation space.

To address these concerns, we additionally simulate performance using the approximate planar boundaries used in (19) with quantization error from ADCs of varying precisions. These planar decision boundaries form decision regions that are intersections of half-spaces, and would be simpler to implement and require less computational overhead than the quadric boundaries. Fig. 8 compares the SER of the 16-ary practical constellation for planar and quadric decision boundaries, with added quantization error from an ADC with $N = 16$, 64, 256, or ∞ equally spaced levels (i.e., an ideal ADC). For the quadric decision boundaries, we find that a $N = 16$ ADC results in a significant performance degradation while a $N = 256$ ADC performs nearly identically to the ideal ADC. With no added quantization error, planar decision boundaries result in a receiver sensitivity gap of approximately 0.3dB from the quadric decision boundaries at $P_{\mathrm{e}} = 4.4 \times 10^{-4}$.

VII. Conclusion

In this paper, we discussed constellation design for ASVD. We derived an approximate SER union bound and an objective function for optimizing ASVD constellations. We described a geometric interpretation of ASVD constellation optimization as a scaled-sphere packing problem. We presented two new methods of constellation design that can be used to find both optimized and practical ASVD constellations. We simulated the performance of new optimized and practical constellations for $M = 2, 4, 8, 16, 32$, and 64, and found that the new constellations outperform or are equivalent to all previously proposed constellations. In particular, we showed improvements of 2.02 and 1.91 dB in receiver sensitivity over the previous best 16-ary and 64-ary constellations. Lastly, we compared the required drive levels of different modulators and simulated the performance degradation with planar decision boundaries and finite ADC precision.

There are still open questions about three-dimensional SV constellations that could be explored in future work. The effects of uncompensated chromatic dispersion or polarization mode dispersion could be explored. Optimal bit mappings for the constellations designed in this paper could be studied, and the constellations could likely be further optimized to minimize the bit-error ratio instead of the symbol-error ratio. Considering systems in which thermal and amplifier noises are of similar magnitudes, we find it intriguing to note that TSVD constellations can be optimized using an equiradial sphere packing [18]. We suspect power-efficient constellations for a mixed noise regime could be found using the packing methods discussed in this paper with a modified sphere radius.

Acknowledgment

The authors are grateful for their discussions with Ethan M. Liang in preparation of the manuscript.

References

[1] S. Betti, F. Curti, G. De Marchis, and E. Iannone, "Multilevel coherent optical system based on Stokes parameters modulation," *J. Lightw. Technol.*, vol. 8, no. 7, pp. 1127–1136, Jul. 1990.

[2] E. Ip, A. P. T. Lau, D. J. F. Barros, and J. M. Kahn, "Coherent detection in optical fiber systems," *Opt. Exp.*, vol. 16, no. 2, pp. 753–791, Jan. 2008.

[3] M. Morsy-Osman et al., "DSP-free 'coherent-lite' transceiver for next generation single wavelength optical intra-datacenter interconnects," *Opt. Exp.*, vol. 26, no. 7, pp. 8890–8903, Apr. 2018.

[4] M. Chagnon, "Optical communications for short reach," *J. Lightw. Technol.*, vol. 37, no. 8, pp. 1779–1797, Apr. 2019.

[5] W. Shieh and H. Ji, "Advanced direct detection schemes," presented at Opt. Fiber Commun. Conf., Washington, DC, USA, Jun. 6–11, 2021, Paper Th4D.5.

[6] K. Kikuchi and S. Kawakami, "Multi-level signaling in the stokes space and its application to large-capacity optical communications," *Opt. Exp.*, vol. 22, no. 7, pp. 7374–7387, 2014.

[7] D. Che, A. Li, X. Chen, Q. Hu, Y. Wang, and W. Shieh, "160-Gb/s stokes vector direct detection for short reach optical communication," presented at Opt. Fiber Commun. Conf., San Francisco, CA, USA, Mar. 9–13, 2014, Paper Th5C.7.

[8] M. Chagnon, M. Osman, D. Patel, V. Veerasubramanian, A. Samani, and D. V. Plant, "1λ, 6 bits/symbol, 280 and 350 Gb/s direct detection transceiver using intensity modulation, polarization multiplexing, and inter-polarization phase modulation," presented at Opt. Fiber Commun. Conf., Los Angeles, CA, USA, Mar. 22–26, 2015, Paper Th5B.2.

[9] P. Dong, X. Chen, K. Kim, S. Chandrasekhar, Y.-K. Chen, and J. H. Sinsky, "128-Gb/s 100-km transmission with direct detection using silicon photonic stokes vector receiver and I/Q modulator," *Opt. Exp.*, vol. 24, no. 13, pp. 14208–14214, Jun. 2016.

[10] T. M. Hoang et al., "Single wavelength 480 Gb/s direct detection over 80 km SSMF enabled by Stokes vector Kramers Kronig transceiver," *Opt. Exp.*, vol. 25, no. 26, pp. 33534–33542, Dec. 2017.

[11] S. Ghosh, Y. Kawabata, T. Tanemura, and Y. Nakano, "Polarization-analyzing circuit on InP for integrated Stokes vector receiver," *Opt. Exp.*, vol. 25, no. 11, pp. 12303–12310, May 2017.

[12] K. Kikuchi, "Sensitivity analyses of Stokes-vector receivers for cubic-lattice polarization modulation," in *Proc. 23rd Opto- Electron. Commun. Conf.*, 2018, pp. 1/2.

[13] T. Hoang et al., "Enabling high-capacity long-reach direct detection transmission with QAM-PAM Stokes vector modulation," *J. Lightw. Technol.*, vol. 36, no. 2, pp. 460–467, Jan. 2018.

[14] D. Che, C. Sun, and W. Shieh, "Optical field recovery in Stokes space," *J. Lightw. Technol.*, vol. 37, no. 2, pp. 451–460, Jan. 2019.

[15] A. Tasbihi and F. R. Kschischang, "Successive four-dimensional Stokes-space direct detection," presented at Opt. Fiber Commun. Conf., San Diego, CA, USA, Mar. 11–15, 2018, Paper W2A.61.

[16] H. Jia, E. Liang, and J. M. Kahn, "Optimal shaping for the stokes vector receiver," *J. Lightw. Technol.*, vol. 41, no. 22, pp. 6884–6897, Nov. 2023.

[17] K. Kikuchi, "Quantum theory of noise in Stokes vector receivers and application to bit error rate analysis," *J. Lightw. Technol.*, vol. 38, no. 12, pp. 3164–3172, Jun. 2020.

[18] M. Morsy-Osman, M. S. Alam, K. A. Shahriar, S. Lessard, and D. V. Plant, "Optimum three-dimensional constellations for Stokes vector direct detect receivers," *IEEE Photon. Technol. Lett.*, vol. 31, no. 8, pp. 587–590, Apr. 2019.

[19] E. Agrell and M. Karlsson, "Power-efficient modulation formats in coherent transmission systems," *J. Lightw. Technol.*, vol. 27, no. 22, pp. 5115–5126, 2009.

[20] I. B. Djordjevic, A. Z. Jovanovic, Z. H. Peric, and T. Wang, "Multi-dimensional optical transport based on optimized vector-quantization-inspired signal constellation design," *IEEE Trans. Commun.*, vol. 62, no. 9, pp. 3262–3273, Sep. 2014.

[21] S. Zhang, F. Yaman, E. Mateo, T. Inoue, K. Nakamura, and Y. Inada, "A generalized pairwise optimization for designing multi-dimensional modulation formats," presented at Opt. Fiber Commun. Conf., Los Angeles, CA, USA, Mar. 19–23, 2017, Paper W4A.6.

[22] F. Kayhan and G. Montorsi, "Constellation design for transmission over nonlinear satellite channels," in *Proc. IEEE Glob. Commun. Conf.*, 2012, pp. 3401–3406.

[23] K. Yan, F. Yang, C. Pan, J. Song, F. Ren, and J. Li, "Genetic algorithm aided gray-APSK constellation optimization," in *Proc. 9th Int. Wireless Commun. Mobile Comput. Conf.*, 2013, pp. 1705–1709.

[24] G. Foschini, R. Gitlin, and S. Weinstein, "Optimization of two-dimensional signal constellations in the presence of Gaussian noise," *IEEE Trans. Commun.*, vol. COM-22, no. 1, pp. 28–38, Jan. 1974.

[25] R. Krishnan, A. Graell i Amat, T. Eriksson, and G. Colavolpe, "Constellation optimization in the presence of strong phase noise," *IEEE Trans. Commun.*, vol. 61, no. 12, pp. 5056–5066, Dec. 2013.

[26] R. R. Borujeny and F. R. Kschischang, "A signal-space distance measure for nondispersive optical fiber," *IEEE Trans. Inf. Theory*, vol. 67, no. 9, pp. 5903–5921, Sep. 2021.

[27] W. Shieh, H. Khodakarami, and D. Che, "Polarization diversity and modulation for high-speed optical communications: Architectures and capacity," *APL Photon.*, vol. 1, no. 4, 2016, Art. no. 040801.

[28] P. Becker, N. Olsson, and J. Simpson, *Erbium-Doped Fiber Amplifiers*. San Diego, CA, USA: Academic Press, 1999.

[29] S. N. Savenkov, "Jones, and Mueller matrices: Structure, symmetry relations, and information content," in *Light Scattering Reviews 4: Single Light Scattering and Radiative Transfer*. Berlin, Germany: Springer, 2009, pp. 71–119.

[30] H. Khodakarami, D. Che, and W. Shieh, "Information capacity of polarization-modulated and directly detected optical systems dominated by amplified spontaneous emission noise," *J. Lightw. Technol.*, vol. 35, no. 14, pp. 2797–2802, Jul. 2017.

[31] J. Proakis and M. Salehi, *Digital Communications*, 5th ed. New York, NY, USA: McGraw-Hill Higher Education, 2008.

[32] S. Benedetto and E. Biglieri, *Principles of Digital Transmission: With Wireless Applications*. Norwell, MA, USA: Kluwer, 1999.

[33] J. H. Conway and N. J. A. Sloane, *Sphere Packings, Lattices and Groups*. New York, NY, USA: Springer, 1999.

[34] N. J. A. Sloane, R. H. Hardin, T. D. S. Duff, and J. H. Conway, "Minimal-energy clusters of hard spheres," *Discrete Comput. Geometry*, vol. 14, no. 3, pp. 237–259, 1995.
[35] N. W. Johnson, *Geometries and Transformations*. Cambridge, U.K.: Cambridge Univ. Press, 2018.
[36] G. D. Forney and L.-F. Wei, "Multidimensional constellations. I. Introduction, figures of merit, and generalized cross constellations," *IEEE J. Sel. Areas Commun.*, vol. 7, no. 6, pp. 877–892, Aug. 1989.
[37] B. Souvignier, "A general introduction to space groups," in *Space-Group Symmetry (Series International Tables for Crystallography)*, 6th ed, M. I. Aroyo, Ed., Hoboken, NJ, USA: Wiley-Blackwell, Dec. 2016, vol. A, pp. 22–41.
[38] *IEEE Standard for Ethernet Amendment 2: Physical Layer Specifications and Management Parameters for 100 Gb/s Operation Over Backplanes and Copper Cables*, IEEE Standard 802.3bj-2014 (Amendment to IEEE Standard 802.3-2012 as amended by IEEE Standard 802.3bk-2013), Sep. 2014.
[39] Y. Che, T. Bo, Y. Yu, and H. Kim, "Coaxial double cubic lattice constellation for Stokes vector direct-detection receiver," in *Proc. OptoElecton. Commun. Conf. & Int. Conf. Photon. Switching Comput.*, Fukuoka, Japan, Jul. 2019, Paper ThC3.2.

Thomas Horton King (Graduate Student Member, IEEE) received the B.S. degree in electrical engineering from Carnegie Mellon University, Pittsburgh, PA, USA, in 2023. He is currently working toward the Ph.D. degree in electrical engineering with Stanford University, Stanford, CA, USA. His research interests include optical communications and coherent data center links.

Joseph M. Kahn (Life Fellow, IEEE) received the A.B., M.A., and Ph.D. degrees in physics from the University of California, Berkeley, CA, USA, in 1981, 1983, and 1986, respectively. During 1987–1990, he was with AT&T Bell Laboratories. In 1989, he demonstrated the first successful synchronous (i.e., coherent) detection using semiconductor lasers, achieving record receiver sensitivity. During 1990–2003, he was with the Electrical Engineering and Computer Sciences Faculty, Berkeley. He demonstrated coherent detection of QPSK in 1992. In 1999, D. S. Shiu and Kahn published the first work on probabilistic shaping for optical communications. In the 1990s and early 2000s, Kahn and collaborators performed seminal work on indoor and outdoor free-space optical communications and multiinput multioutput wireless communications. In 2000, Kahn and K.-P. Ho founded StrataLight Communications, whose 40 Gb/s-per-wavelength long-haul fiber transmission systems were deployed widely by AT&T, Deutsche Telekom, and other carriers. In 2002, Ho and Kahn applied to patent the first electronic compensation of fiber Kerr nonlinearity. StrataLight was acquired by Opnext in 2009. In 2003, he became a Professor of electrical engineering with E. L. Ginzton Laboratory, Stanford University. Kahn and collaborators have extensively studied rate-adaptive coding and modulation, and digital signal processing for mitigating linear and nonlinear impairments in coherent systems. In 2008, E. Ip and Kahn (and G. Li independently) invented simplified digital backpropagation for compensating fiber Kerr nonlinearity and dispersion. Since 2004, Kahn and collaborators have studied propagation, modal statistics, spatial multiplexing and imaging in multimode fibers, elucidating principal modes and demonstrating transmission beyond the traditional bandwidth-distance limit in 2005, deriving the statistics of coupled modal group delays and gains in 2011, and deriving resolution limits for imaging in 2013. His research interests include optical frequency comb generators, coherent data center links, rate-adaptive access networks, fiber Kerr nonlinearity mitigation, ultra-long-haul submarine links, and optimal free-space transmission through atmospheric turbulence. He was the recipient of the National Science Foundation Presidential Young Investigator Award in 1991.